ACS APPLIED MATERIALS & INTERFACES

Research Article

www.acsami.org

Real-Time Monitoring of Post-Surgical and Post-Traumatic Eye Injuries Using Multilayered Electrical Biosensor Chip

Muhammad S. Khan,[†,⊥] Santosh K. Misra,[†,⊥] Aaron S. Schwartz-Duval,[†,⊥] Enrique Daza,[†,⊥] Fatemeh Ostadhossein,[†,⊥] Matthew Bowman,[∥] Akshay Jain,[#] Gina Taylor,[∥] Deana McDonagh,[∥] Leanne T. Labriola,[#,%] and Dipanjan Pan*[,†,⊥,‡,§,#]

[†]Department of Bioengineering, [‡]Beckman Institute for Advanced Science and Technology, [§]Department of Materials Science and Engineering, and [∥]School of Art and Design, University of Illinois at Urbana−Champaign, Urbana, Illinois 61801, United States

[⊥]Biomedical Research Center and [#]Ophthalmology, Carle Foundation Hospital, Urbana, Illinois 61801, United States

[%]Department of Surgery, University of Illinois College of Medicine, Urbana, Illinois 61801, United States

Supporting Information

ABSTRACT: Lack of current techniques for the early monitoring of bleb leaks and other post-traumatic or post-surgical ocular injury has posed an unmet clinical need for the development of new techniques. Present evaluation techniques use either subjective or nonquantitative approaches. At present, there are no FDA approved ocular devices that can directly measure ascorbic acid (AA) concentration levels for both tear film (TF) and aqueous humor (AH) at point-of-care (POC) level. Toward this aim, we present a novel POC quantitative assay, called the ocular biosensor device, which can be used to evaluate the integrity of the anterior surface of the eye by measuring the concentration of AA in TF and AH. Herein, we utilize a novel scientific engineering approach for the development of a disposable paper based POC ocular biosensor strip. A grafted poly(styrene)-*block*-poly(acrylic acid) (PS-*b*-PAA) and graphene platelet composite with contour based μ-electrodes design (CBμE) exhibit a highly sensitive platform to perform electrochemical immunosensing technique to study clinical samples that have small volumes like tear fluid. Samples used in this study were collected clinically from subjects undergoing therapeutic anterior chamber paracentesis. The proposed biosensor reports the level of AA concentration on an electronic screen, making the results easy to read, efficient, and reliable.

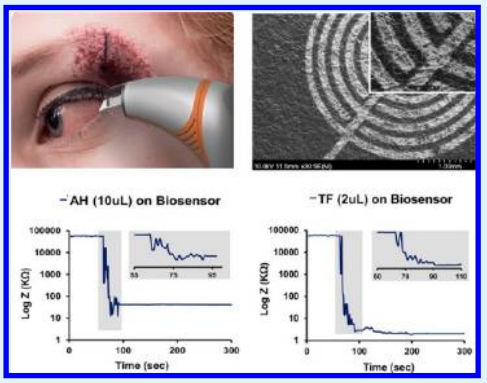

KEYWORDS: *eye injury, glaucoma, point-of-care, biosensor, graphene, tear film, aqueous humor, ascorbic acid, ascorbate oxidase*

1. INTRODUCTION

Glaucoma is reported to affect 3.4 million people over the age of 40 years in USA.[1−11] The number one surgical treatment for glaucoma is a filtering procedure called a trabeculectomy. This treatment lowers intraocular pressure (IOP) from uncontrolled glaucoma[12] by shunting aqueous fluid outside of the eye into the subtenon's space through an anterior scleral incision. This creates an external reservoir of fluid called an encapsulated bleb and allows aqueous humor (AH) to bypass the typical drainage system through the trabecular meshwork.[13] However, 14% of cases have reported complication from this procedure due to a wound leak.[5,14,15] A wound leak can then lead to infection which can threaten vision. It is estimated that 41−45% of patients who suffer from a bleb-related infection will have severe vision loss of 20/400 or worse.[7,9] Therefore, many other reports stress the importance of vigilance in monitoring post-trabeculectomy patients.[8,12] Timely diagnosis and early treatment to correct leaks are critical.[5] Currently, one of the most commonly used methods to evaluate these wounds involves the use of an office technique called the Seidel test.[4,16] In this test, fluorescein dye is placed onto the ocular surface, and a trained physician observes the eye for a change in color that would represent a wound leak from the passage of AH through the wound. The Seidel test is subjective, not standardized, and the amount of pressure during the technique varies between clinicians.[3]

The surface of the eye is sensitive which needs to be kept moist. The eyes are in constant contact of eyelids. Without lubrication, the friction between the two layers of conjunctiva would cause rubbing. To prevent this, and to help remove debris, eye produces a tear film. Tear film is essential in maintaining ocular homeostasis and monitoring ocular surface conditions.[17] The tear fluid secreted by the lacrimal glands is a complex matrix comprising of an inner mucin layer, middle aqueous layer, and the outer lipid layer as shown in Figure 1A. The composition of tear film included lipids, proteins, peptides, proteases, protease inhibitors, and metabolites.[18] Tear film is separated from aqueous humor by cornea. Aqueous humor, rich

Received: February 3, 2017
Accepted: February 16, 2017
Published: February 16, 2017

DOI: 10.1021/acsami.7b01675
ACS Appl. Mater. Interfaces 2017, 9, 8609−8622

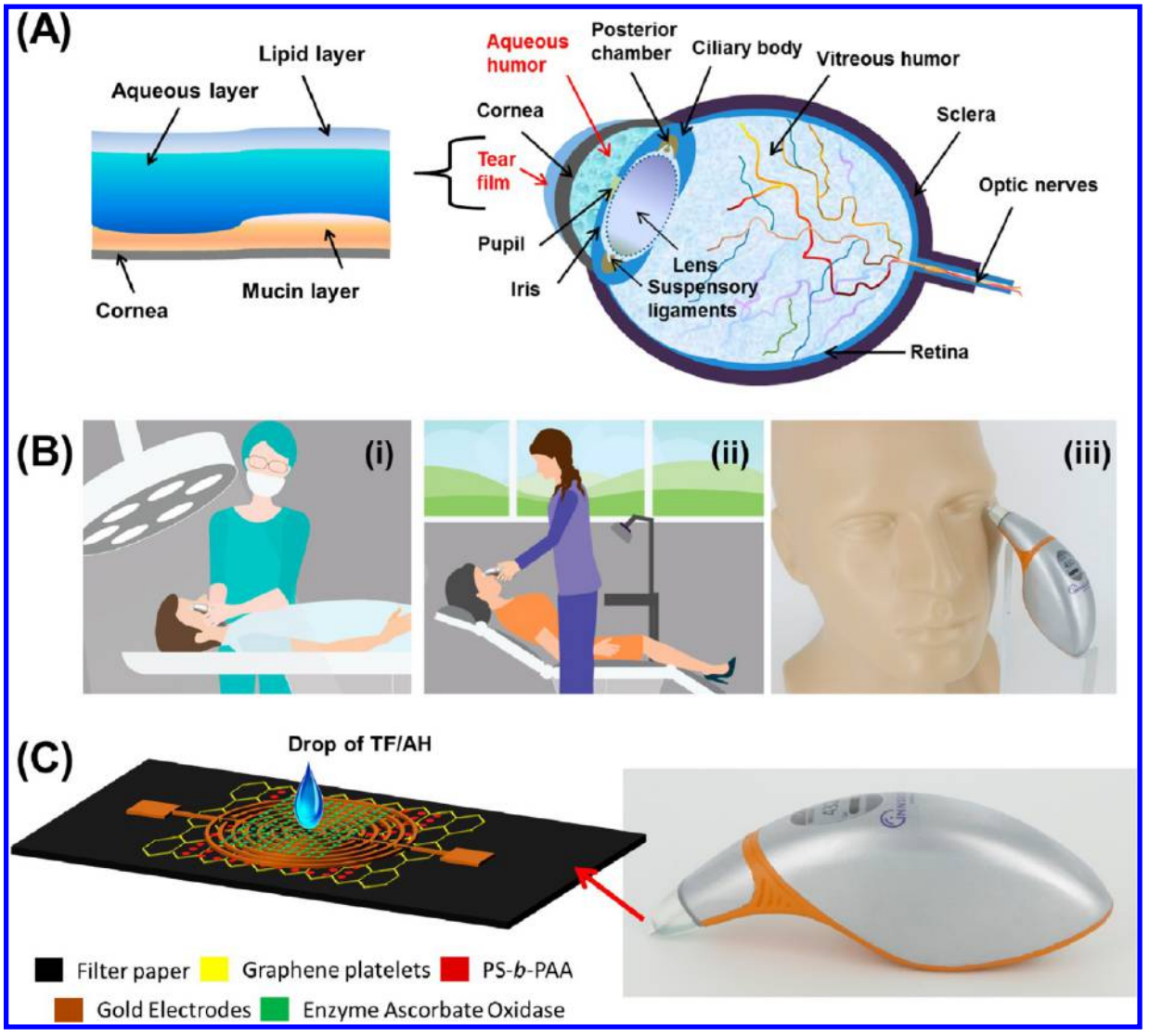

Figure 1. Clinical impact of the ocular device and the biosensor chip. (A) Right: graphical representation of the anatomy of eye revealing the relative location of aqueous humor, and tear film. Left: pictorial description of individual layer in tear fluid. (B) Demonstration of the ocular biosensor device in real-time settings for patients undergoing (i) postsurgery follow-up, (ii) clinical setting, and (iii) mode of tear film sample collection in clinical setting. (C) Schematic representation of biosensor strip and its location in proposed hand-held probe.

in ascorbic acid, is produced continuously, and it circulates through the front part of the eye and then drains away through an area called the trabecular meshwork, near the base of the iris as shown in Figure 1A (right). We hypothesize that the leakage from damaged corneal cells would result in release of ascorbic acids into the tears, which can be directly correlated with the degree of injury. Published analytical assessment of ocular fluids shows an approximate 5-fold difference in the concentration of vitamin C (ascorbic acid) between the AH and tear film (TF). We hypothesize that when the integrity of the anterior globe is disturbed from a full thickness incision or laceration, the higher concentrations of AA from within the continuously produced AH will be released into the TF, causing a rise in the amount of AA in the TF that can easily be quantified with a POC device. The most common methods used to detect ascorbic acid (AA) level in the laboratory include fluorescence,[19] colorimetric,[20−23] HPLC,[24−27] and electrochemical measurements.[28−35] But almost all of these methods suffer from serious limitations such as low concentration detection, obligation to have sophisticated instrumentation, and extensive sample preparations. In this work, we developed, for the first time, a quantitative, robust, and facile-to-operate engineering approach based on nanotechnology for real-time monitoring and detection of AA within the ocular TF. We present the use of AA as a surrogate biomarker to an anterior scleral or corneal wound leak, which could replace the subjective Seidel test. This novel solution to identify the bleb leaks operates using an ocular biosensor hand-held device which provides easy to read result on its screen after a sample tear film collection from placement of the edge of the biosensor strip directly into the tear film meniscus. This test can be easily done by a technician or nurse who could save time for the ophthalmologist because the results and diagnosis of the wound leak will be available to the physician before the actual examination.

In the clinic, the two most common methods used to collect the TF sample are glass capillary tubes[36,37] and Schirmer stripes.[38−40] Schirmer strips are invasive, and because of the small volume collected, it is difficult to detect the AA accurately.[41] Additionally, due to the invasive nature of Schirmer strip usage, there exists potential for either

DOI: 10.1021/acsami.7b01675
ACS Appl. Mater. Interfaces 2017, 9, 8609−8622

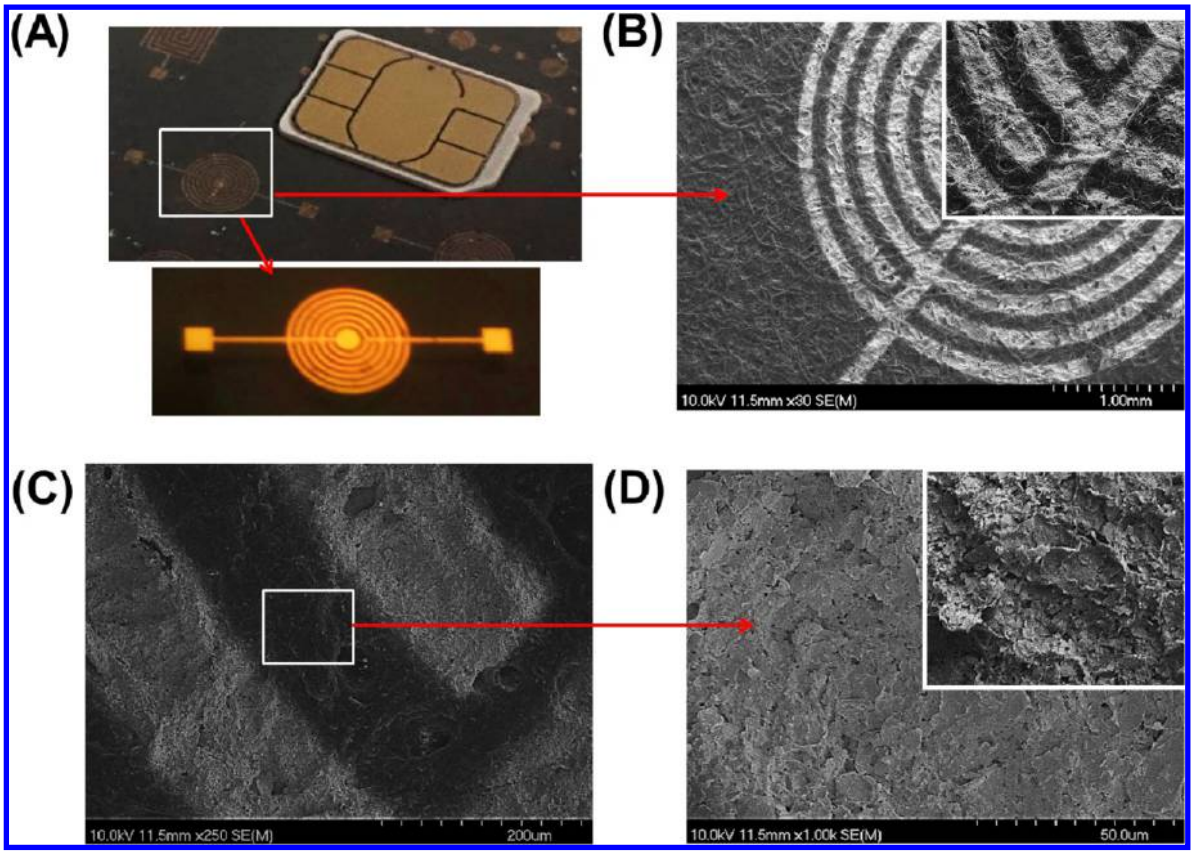

Figure 2. High-resolution imaging of the developed ocular biosensor chip. (A) Optical image of the sensing area. A nano sim card is displayed along with the fabricated chip for size reference only. (B) SEM image of sensing area in biosensor chip after treating ascorbate oxidase enzyme on the surface. (C) Area represents the interspacing between two Au electrodes of 40 nm thickness, 50 nm width, and 50 nm interspacing. (D) Highlighted area represents the spin-coated graphene−polymer after deposition of Au electrodes. Insets of (B) and (D) revealed the detailed surface morphology of fabricated Au electrodes and spin-coated graphene−polymer on filter paper.

transudation of vascular fluid or leakage from damaged cells at the site of collection, both of which could lead to a significant increase in AA concentration. Another possible reason for high AA could be due to the presence of corneal epithelial cells in tear film during leakage, since these cells also have high AA concentration.[42,43] The capillary tube method for collecting tear film is much less invasive compared to Schirmer strip collection. The technique presented in this work utilizes a multilayered design with graphene platelets at its core for their excellent electrical and thermal conducting properties while acting as an effective barrier to form a 2-dimensional functional surface. Graphene nanoplatelets provide multifunctional properties (electrical, thermal, physical) with "platelet" morphology of thin (~6−8 nm) but wide aspect ratio (~25 μm). The choice of this material is deliberate since the pure graphitic composition will impart excellent electrical and thermal conducting properties and simultaneously be effective at providing barrier properties. In order to achieve a selective and highly specific biological recognition of AA, ascorbate oxidase (AO) enzyme is placed on the graphene platelets with an amphiphilic diblock copolymer, poly(styrene)-*block*-poly(acrylic acid) (PS-*b*-PAA), used a bridge. The noncovalent $\pi-\pi$ stacking interaction between the two-dimensional graphene platelets comprising phenyl groups and multiple repeat units of poly(1-phenylethylene) functionalities of the diblock copolymer could be realized. The acrylic acid residues at the top of this bilayered arrangement enable stable immobilization with the enzymes. We anticipate that the highly specific molecular recognition between AA and the enzyme ascorbic oxidase will produce a change in resistance upon their interaction, which can be measured with an impedance-based detector, suggesting that the disposable sensor chip can be designed to measure the AA in clinical settings by measuring this change in resistance using a hand-held multimeter.

A low-cost ocular biosensor strip was developed by spin-coating the filter paper with a thin layer of composite containing PS-*b*-PAA and graphene platelets (GP). CBμE design was developed and fabricated on hybrid GP composite using electron-beam evaporator. Sensing area was then coated with enzyme AO to make the POC biosensor ready for AA measurements. Our method of using an electrical resistance based biosensor offers high sensitivity for AA detections in small volumes of TF and AH. Extensive characterizations were performed to validate the layer-by-layer interaction of the ocular biosensor strip and its successful development. The resistance-based measurement provided by the sensor can be easily performed in the clinical setting with immediate results without having to outsource analysis, as competing assays would require.

2. RESULTS AND DISCUSSION

Concept and Design. A hand-held device with ocular biosensing capabilities was aimed to achieve through composition of multilayer sensing platform and structure crafting using specialized scientific techniques of nanotechnology and sophisticated assembly using industrial engineering

DOI: 10.1021/acsami.7b01675
ACS Appl. Mater. Interfaces 2017, 9, 8609−8622

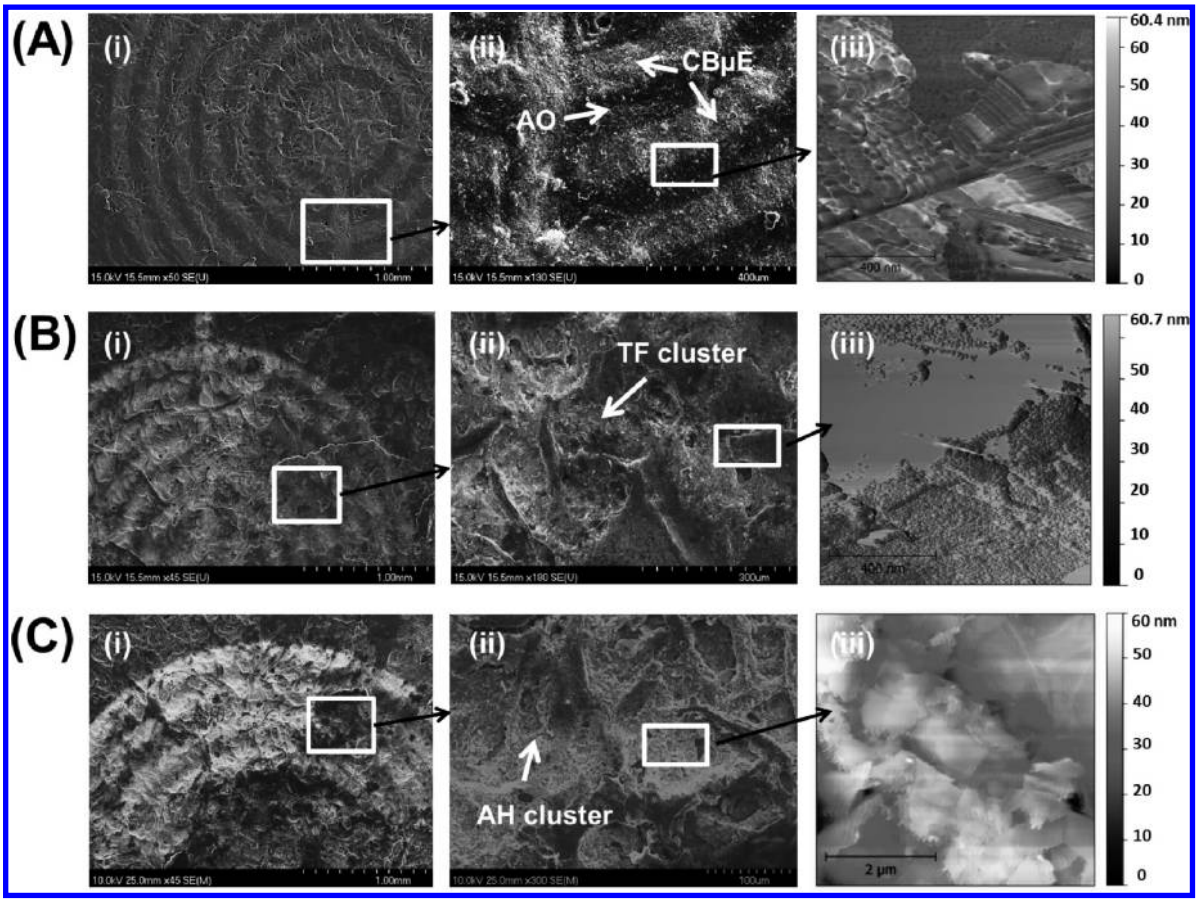

Figure 3. Morphological and topographical investigation of fabricated CBμE design on GP composite after sensing of TF and AH samples. SEM (i, ii) and AFM (iii) imaging of used ocular biosensor strips. (A) AO enzyme immobilized on sensing area with scale bar i: 1 mm; ii: 400 μm; iii: 400 nm. (B) TF sample (2 μL) loaded on sensing area with scale bar i: 1 mm; ii: 300 μm; iii: 400 nm. (C) AH sample (5 μL) loaded on sensing area with scale bar i: 1 mm; ii: 100 μm; iii: 2 μm.

approach. To understand the user needs and expectations of the ocular biosensor device, optimization of design was performed to produce a simple device with a more practical design to operate easily in a clinical setting. One of the primary considerations was the position in which the device would need to be held in order to perform its operation successfully. Figure 1B describes three possible situations (OR (post-trauma or postsurgical setting), clinical setting, and tear film collection) for its application. As the action for our product would require similar tests and applications; therefore, the proposed ocular biosensor device was integrated into the design as shown in Figure 1C. The biosensor strip was then inserted at the desired location to perform detection of AA concentration in TF. The biosensor strip was composed of filter paper coated with thin layer of graphene−polymer, Au electrodes, and ascorbate oxidase enzyme.

Production of Base Layer of Biosensor. Base material for the proposed ocular biosensor chip was produced by spin-coating the composite of graphene nanoplatelets and PS-*b*-PAA (GP) over Whatman filter paper. Spin-coating (Figure S1a) was attempted on filter papers of both the sizes of 5 and 7 cm. However, issues were encountered with the bigger size of paper (7 cm). The spin-coat instrument did not hold the paper firmly, and consequently vacuum was not obtained. As a result of this only filter paper of 5 cm was used for subsequent studies. The GP (0.1 mg/mL) composite with ratio 10:1 of graphene and polymer was spun at 200 rpm for 60 s followed by 500 rpm for 85 s. Suspension was poured on filter paper during first cycle of rotation of 200 rpm. Figure 2B shows the SEM image of the spin-coated GP layer on the filter paper. Figure S1c shows unevenly distributed graphene−polymer on filter paper (5 cm) using the drop-cast method. Both samples were dried using a nitrogen spray gun for 5 min and were further dried overnight under hood at room temperature under germ-free conditions.

Fabrication of Contour Based μ-Electrode. A contour based μ-electrode (CBμE) was generated as an innovative design configuration to achieve better accuracy for handling samples with small volumes. The small electrode setup was a key step to the fabrication of the sensor chip. CBμE design (shape) was introduced to increase the sensitivity and dynamic range of the sensing mechanism. Electron beam evaporator was used for the production of CBμE using a shadow mask directly on thin layer of GP composite. This configuration ensures high conductivity for stable electrical signals transfer within actual sensing area of 1.5 mm × 1.5 mm. It follows surrounding sensing environment with less baseline capacitance. Scanning electron microscopy (SEM) was employed to characterize the surface morphology of the evaporated electrodes as shown in Figure 2B,C.

Immobilization of Ascorbate Oxidase Enzyme. Specificity of the ocular biosensor chip to detect AA was achieved by introducing ascorbate oxidase (AO) enzyme onto the hybrid graphene−polymer coating with plated CBμE on it as shown in Figure S2. Immobilization of the enzymes on the solid surfaces

DOI: 10.1021/acsami.7b01675
ACS Appl. Mater. Interfaces 2017, 9, 8609−8622

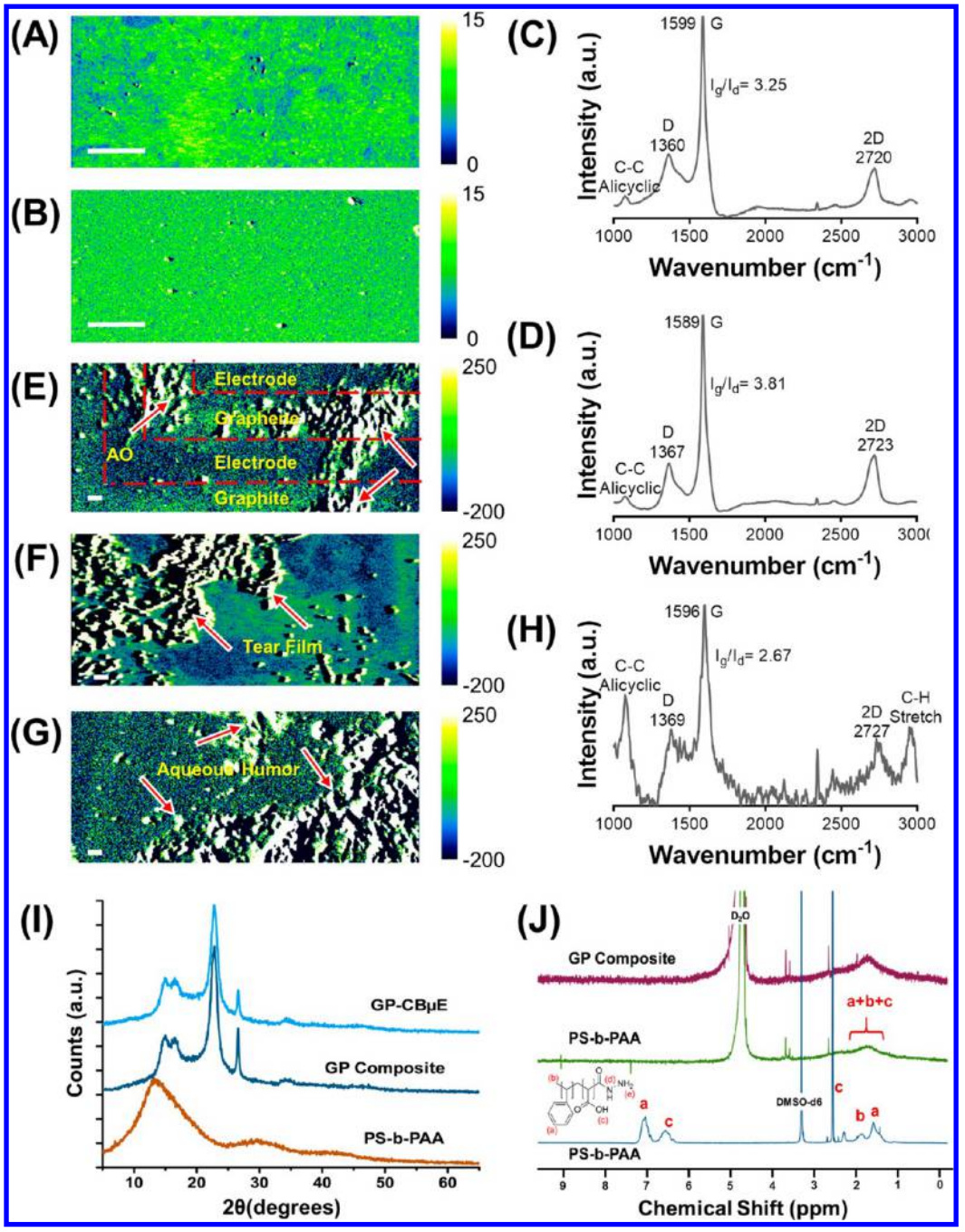

Figure 4. Raman spectroscopic, XRD, and NMR analysis of layer-by-layer characterization of the fabricated biosensor chip. (A) A Raman generated intensity heat map of a graphene−polymer decorated surface, spin-coated at 350 rpm, and (B) 200 rpm (20× objective). (C) Raman generated spectral analysis of intensity heat map of a graphene−polymer decorated surface, spin-coated at 350 rpm labeled with respective chemical peak associations. (D) Raman generated spectral analysis of intensity heat map of a graphene−polymer decorated surface, spin-coated at 200 rpm labeled with respective chemical peak associations. (E) Raman generated intensity heat map of ascorbate oxidase (AO) layering on graphene−polymer decorated surface. Areas with gold electrode strips are labeled as electrode, while AO clusters are indicated by red arrows. (F) Raman generated intensity heat map of tear film (TF) and (G) aqueous humor (AH) sample on AO−graphene−polymer decorated surface. TF and AH clusters are indicated by red arrows. (H) Raman spectral analysis of AH corresponding to (G) and labeled with respective chemical peak associations. (All heat maps were measured at 1600 cm^{-1}; color bar indicates intensity value per pixel; scale bar: 100 μm). (I) X-ray diffraction patterns of PS-*b*-PAA, GP, and the electrode. XRD was utilized to characterize the layered structure of the biosensor strips. (J) Chemical characterization through ^{1}H NMR spectroscopy (blue) PS-*b*-PAA in DMSO-d_6; (green) PS-*b*-PAA in D_2O; (purple) after the incorporation of graphene−nanoplatelets in polymer.

can be achieved using a large variety of physical and chemical methods including one of the most important by adsorption. This utilizes the physical interactions occurring between the surface functional groups and enzyme that include van der Waals forces, ionic interactions, and hydrogen bonding.[44] The presence of acrylic acid residues in the PS-*b*-PAA polymer ensures such weak interactions to hold enzyme AO on the surface of the sensor without changing the native structure of the enzyme involving one or all of these interactions. The acrylic acid ($-CO_2H$) residues of the diblock copolymer were

DOI: 10.1021/acsami.7b01675
ACS Appl. Mater. Interfaces 2017, 9, 8609−8622

supposedly involved in facile immobilization of the AO enzyme on the composite layer of GP. We anticipate that the specific interaction of AA with AO will produce a difference in the resistance of the biosensor chip, which can easily be measured by electrochemical potentiostat. The structural features of ocular biosensor chip were further characterized using SEM and AFM before and after immobilization of AO enzyme as shown in Figure 3A. After AO immobilization on the allocated sensing area of the sensor chip, polymer contents from GP layer found to be physically interacting with AO as illustrated in Figure 3Aii. The image was captured after 3 h of AO immobilization on the sensor area. It was revealed that AO was uniformly distributed on GP composite. However, some AO contents were also coated on CBμE plates as magnified using AFM in Figure 3Aiii. To further elaborate the interface testing of the AO enzyme with real samples, 2 μL of TF and 5 μL of AH were tested as shown in Figures 3B and 3C, respectively. Cluster of TF (Figure 3Bii) and AH (Figure 3Cii) shows colocalization of AO enzyme with GP composite. AFM was further used to visualize the surface topology at high resolution (1×1 μm^2). It was observed that TF with a low volume of 2 μL (65.7 nm) associated progressively as compared to AH with a volume of 5 μL (600 nm) as shown in Figures 3Biii and 3Ciii, respectively. The high height profile of AH was because of the large sample volume tested on the sensor strip. To further elaborate the interactions between AO-TF and AO-AH, the biosensor strips were additionally investigated using Raman spectroscopy.

The chemical composition and surface chemistry of the biosensor play a very specific role for accurate enzyme functionalization and subsequent TF or AH analysis. Additionally, a graphitic passivation could ensure the electrical and thermal conducting properties surrounding the ion beam deposited gold electrode.[45]

Raman Analysis and Imaging. To evaluate chemical composition and surface chemistry of post-AA sensing in AH or TF, Raman characterization was performed on various pretreated biosensor chips so as to determine bond chemistry as well as compare the presence of AO, TF, and AH to the graphene−polymer (GP) decorated surface. Initially, two separate spin-coating approaches of the GP material were investigated to yield an even and highly graphitic-based passivation. A Raman intensity heat map of a sample spun at 350 rpm was imaged at 1600 cm^{-1} (the characteristic graphene wavenumber) and unveiled a highly uneven distribution of the graphene nanoplatelets in GP composite as shown in Figure 4A. A sample spun at 200 rpm revealed a more even coating (Figure 4B). Raman spectral analysis of the graphitic band (G) (indicating sp^2 hybridization) and the diamond band (D) (indicating sp^3 hybridization)[46] was used to quantify the observed difference in graphite−polymer passivation. Between the two speed formulations, the 350 rpm sample showed a higher G band wavenumber and a lower G and D band intensity ratio (I_G/I_D ratio) (Figure 4C) as compared to the 200 rpm sample (Figure 4D). It is well-known that as graphene layers' increase, the G band position decreases in wavenumber, while the I_G/I_D ratio also increases. This change was due to the increased number of $\pi-\pi$ interactions caused by graphene stacking[47] as well as poly(styrene)−graphene platelet interactions.[48] This shift in G band and I_G/I_D ratio indicates that the 200 rpm sample is retaining more material and is thus the superior candidate for biosensor fabrication. The AO enzyme is assumed to interact with the poly(acrylic acid) residues of the amphiphilic polymer. Thus, the enzyme should remain between gold ring electrodes to close the circuit by forming a bridge across the positive and negative leads. A Raman generated micrograph of the biosensors' circuitry, post-AO layering, confirmed that the enzyme tended to group on the graphene−polymer material between the gold electrodes (Figure 4E). The enzyme produced much higher signal intensity when compared to the graphene−polymer background (scale bars increased 17-fold). This high intensity signal can be explained through the scarce presence of fluorescent amino acid residues[49] composing AO's protein structure (11.2% abundance): phenylalanine: 4.5%; tyrosine: 4.2%; and tryptophan: 2.5%.[50] Although the fluorescent amino acid composition is minimal, the high intensity contrast between the biological material and the sensor surface enables a clear identification between the two. Next, an ocular tear film sample was added to the sensor and reimaged (Figure 4F). The Raman intensity heat map showed that the tear film contents formed a larger number of clusters than the AO alone, which provided an overall even distribution of high-intensity Raman signals. This combined presence of AO and residual fluorescent amino acids found in TF proteins[51] is further supported since high signal intensity clumps are found on and off the gold electrode, whereas the AO tends to adhere to the graphene only. Similarly, a Raman intensity heat map image of the AO layered sensor treated with AH displayed large clusters of proteins creating high-intensity fluorescent signals (Figure 4G). Raman spectroscopic analysis of AH (Figure 4H) and TF (Figure S3) samples present on the sensor both displayed a new peak characteristic for C−H stretching (2950 cm^{-1} for AH and 2947 cm^{-1} for TF). Since the sensor's graphene platelets and polymer have low instances of C−H bonds, this additional peak is therefore a consequence of the added biological material. Further spectral analysis shows that these samples decrease greatly in their I_G/I_D ratios (2.67 for AH and 2.00 for TF), indicating that the biological material is interacting with the sensor's surface enough to cause a decrease in the graphitic signal integrity. These significant spectral changes define the core attributes necessary for a properly functioning sensor.

X-ray Diffraction. X-ray diffraction (XRD) patterns of PS-*b*-PAA and graphene (GR) nanoplatelet composite were studied to further investigate and assembly of the layer-by-layer (down-to-top) of the proposed ocular biosensor strip. From the pattern, as shown in Figure 4I, it is clear that the presence of GR nanoplatelet led to the appearance of new peaks at 2θ = 22.8° and 26.6° which is attributed to the GR while the broad peak at around 13.5° is shifted to higher values demonstrating the decrease in the *d*-spacing. CBμE grafted on GP composite neither significantly change the spectrum nor generated new peaks. This confirms the presence of uniform spin-coated thin layer of GP composite between electrodes and also due to rapid quenching rate of gold upon condensation on the substrate. Therefore, this results in the formation of metastable amorphous gold layer, which led to the masking by the signature peaks of GR platelets.

Nuclear Magnetic Resonance. ^{1}H NMR spectroscopy was used to determine the chemical structures and detecting the possible chemical interactions between AA and AO. Experiment was performed on a 500 MHz machine. ^{1}H NMR spectroscopy was carried out for PS-*b*-PAA before and after GR incorporation in the matrix as illustrated in Figure 4J. The peak assignment of PS-*b*-PAA was executed accordingly where the chemical shifts at ca. 1.3−1.8 ppm could mainly be attributed to the aliphatic protons from both acrylic acid and

DOI: 10.1021/acsami.7b01675
ACS Appl. Mater. Interfaces 2017, 9, 8609−8622

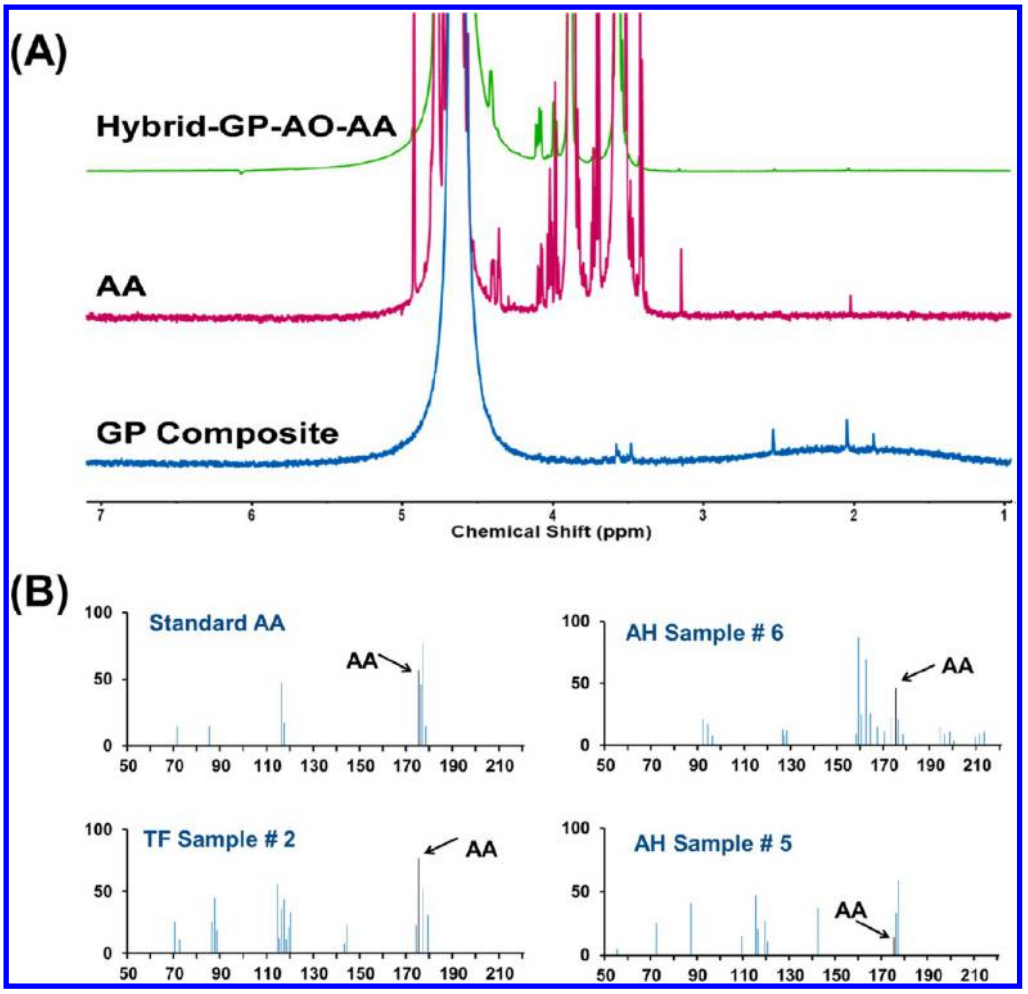

Figure 5. [1]H NMR spectroscopy and HR mass spectrometry to confirm the presence of AA in the samples used for testing. (A) Fragmented AA data reveals the presence of AA with AO immobilized on GP composite. (B) The presence of AA in clinically collected samples (AH and TF) and standard AA sample. The characteristic AA fragment is obtained at m/z of 175.024 (denoted by arrow) in all samples confirming the presence of AA.

polystyrene blocks. In addition, [1]H NMR spectroscopy was also employed to probe AO after deposition onto the GP composite. The highlighted regions represent the retained peaks from AO in the hybrid system, which successfully represent that the AO can generate active sites for interaction with AA for the potential enzymatic reaction as shown in Figure 5A. The AA's peaks were subsequently assigned. In addition to the AA's characteristic peaks, two doublet peaks appeared at 4.01−4.06 ppm as well as a multiplet at 4.13−4.17 ppm as shown in Figure S5a. This could be originating from the fragmented AA after exposure to AO.

Mass Spectrometry and Confirmation of AA Presence. High-resolution mass spectrometry (HR-MS) was used to ensure the presence of AA in the clinically collected samples of AH and TF. The AA identification in the unknown sample was performed through ionization of samples with subsequent analysis of the ions. Produced fragment ions were used to identify the parent molecule and matched to AA on the basis of their mass to charge ratio (m/z). The characteristic AA fragment was measured to be about 175.0242 (m/z) as shown in Figure 5B. It validates the presence of AA in collected clinical AH and TF samples and guaranteed the response in ocular biosensor due to AA present in AH samples. It also supported that the proposed ocular biosensor would offer the impartial standard for categorizing the nature of a wound leak.

X-ray Photoluminescent Spectrum. The peaks for XPS are assigned for the carbon narrow scan where the sp^2 and sp^3 carbon are observed originating from polymer backbone and graphite platelets in the sample in both Figure 6 and Figure 7. In addition, as could be seen in Figure 7, after the addition of AA to the chip, the disulfide bonds available in the protein potentially in aqueous humor or AO have undergone change compared to the original sample (Figure 6), suggesting that the expected change has occurred after the addition of AA on the sample. In addition, other changes in the peak positions are observed on the N 1s peak after the addition of AA as could be seen in Figure S6.

Real-Time Monitoring and Detection of Ascorbic Acid. An electrochemical analyzer CHI 760E (CH Instruments, Austin, TX) potentiostat connected to a computer with the CHI 760E software package was used for all electrochemical measurements. Potentiostat with three electrodes configuration (working electrode, counter electrode, and reference electrode) was connected to biosensor chip terminals to estimate the concentration of AA in the AH and TF clinical samples. Contour electrode and reference electrode attached together to one terminal of the sensor electrode pad and working electrode connected to the other terminal of the biosensor pad as shown in Figure S2a. Initially, the impedance of a thin layer of graphene−polymer (GP) composite on paper-

DOI: 10.1021/acsami.7b01675
ACS Appl. Mater. Interfaces 2017, 9, 8609−8622

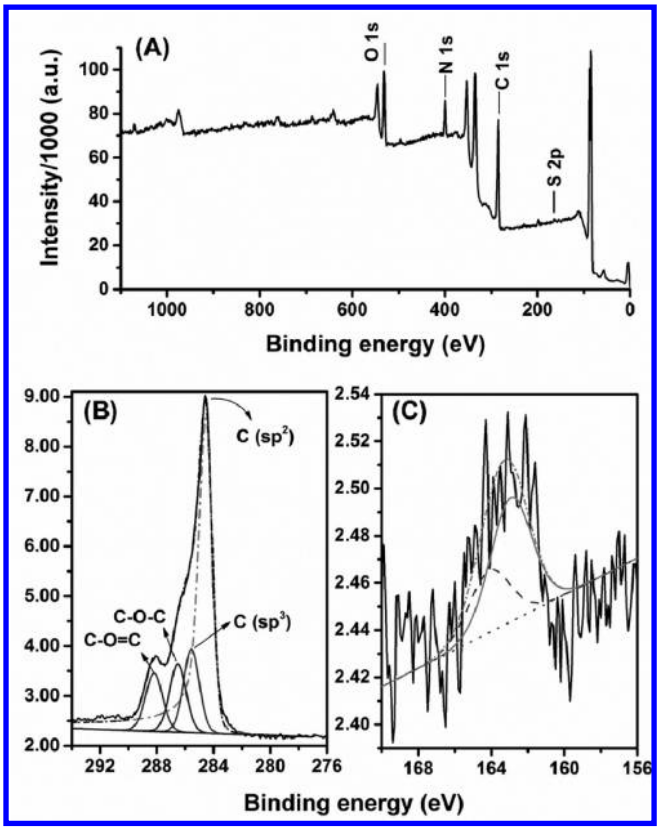

Figure 6. XPS spectrum of the unused sensor deposited with AO enzyme: (A) survey spectrum; (B, C) the narrow scan of C and S, respectively.

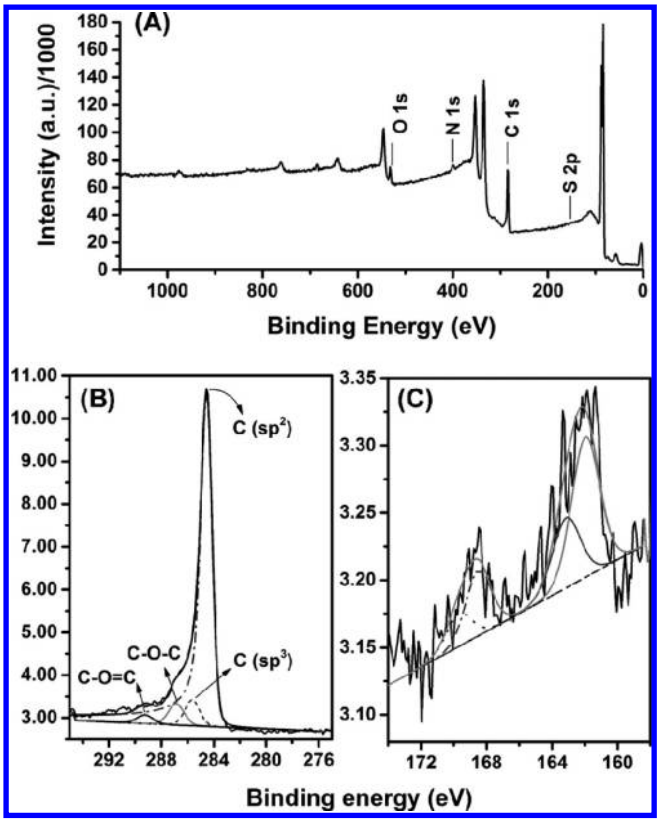

Figure 7. XPS spectrum of the used sensor deposited with AO enzyme with aqueous humor added: (A) survey spectrum; (B, C) the narrow scan of C and S, respectively.

based substrate was measured to be 5.1 ± 0.23 MΩ (n = 21, n is the number of biosensor chip analyzed). After depositing pattern of gold electrodes (CBμE) on base material of GP composite, the impedance decreased to 3.45 ± 0.12 MΩ. The reason for the decrease of impedance was probably the parallel arrangement of CBμE with GP composite. Ascorbic oxidase (AO) enzyme of 5 μL was then electrochemically transduced using drop-cast method directly on the sensing area of the developed biosensor chip. After being coated with enzyme, the PS-*b*-PAA content from GP composite interacted gradually with enzyme and created an interacting association between GR, PS-*b*-PAA and AO in same order. This thread of interactions generated the required platform for a future sample (TF/AH) investigation. This resulted in increased impedance from 3.45 ± 0.12 to 5.5 ± 0.06 MΩ.

To investigate the real time monitoring of both AH and TF samples, disposable paper-based biosensor chip immobilized with AO was assembled carefully in faraday cage to minimize the signal-to-noise ratio (SNR), and the sensor was connected with potentiostat for electrical measurement as shown in Figure S2a. After treating clinical samples with AO, the PS-*b*-PAA regained its interaction with graphene. This allowed AO to react instantaneously with the testing sample at close proximity.

Quantification of AA in Tear Film. Figure 8A reveals the real-time monitoring of electrical impedance response of biosensor strip once the tear sample interacts with ocular biosensor strip. Tear film samples are usually available low in volume, and it varies from person to person. This led us to use of different volumes of TF (0.4, 1, and 2 μL) in real-time fashion to estimate the operating behavior of fabricated biosensor chip at point-of-care (POC) level. Sensor exhibited a different trend in resistivity based on increasing the volume of the tear film. We initially tested low amount (0.4 μL) and then gradually increased the volume to 1 μL and finally 2 μL. Incremental step in volume was only done once we achieved the stable (steady-state) electrical response of the biosensor chip. Ocular biosensor chip developed in this work is completely stable and works efficiently. As shown in Figure 8A, impedance of biosensor decreased from 5.5 ± 0.06 to 1.59 ± 0.04 MΩ after dropping 0.4 μL volume of TF directly on the AO enzyme (5 μL) immobilized biosensor strip. After achieving the steady state electrical response from the system, an additional 0.6 μL was added to make the final volume to 1 μL. At this stage, the impedance of 43.2 ± 0.41 KΩ was recorded and monitored until the sensor achieved the steady state response (at t = 350 s). Finally, the total volume of 2 μL was monitored during 350−600 s with impedance value of 5.1 ± 0.26 KΩ. It is noted that impedance of developed ocular biosensor strip decreased with the addition of TF sample at different loading volumes. Insets of Figure 8A further elaborate the presence of TF on sensor strip and its stability in terms of change in impedance with respect to time. Initially, biosensor chip required only ∼20 s for the coated AO enzyme to completely react with the loaded sample of TR with volume of 0.4 μL. However, with increased volume from 0.4 to 1 μL, sensor gained its linearity after 65 s. In final phase, TF with total volume of 2 μL was monitored and the biosensor strip achieved its stability in less than 90 s. This reveals that ocular biosensor has high probability (>0.95, n = 11) to achieve stabilization reading in less than 60 s with the sample volume of 0.5 to 1 μL and required about 90 s for the sample volume ranging from 1 to 2 μL. These results were acquired during

DOI: 10.1021/acsami.7b01675
ACS Appl. Mater. Interfaces 2017, 9, 8609−8622

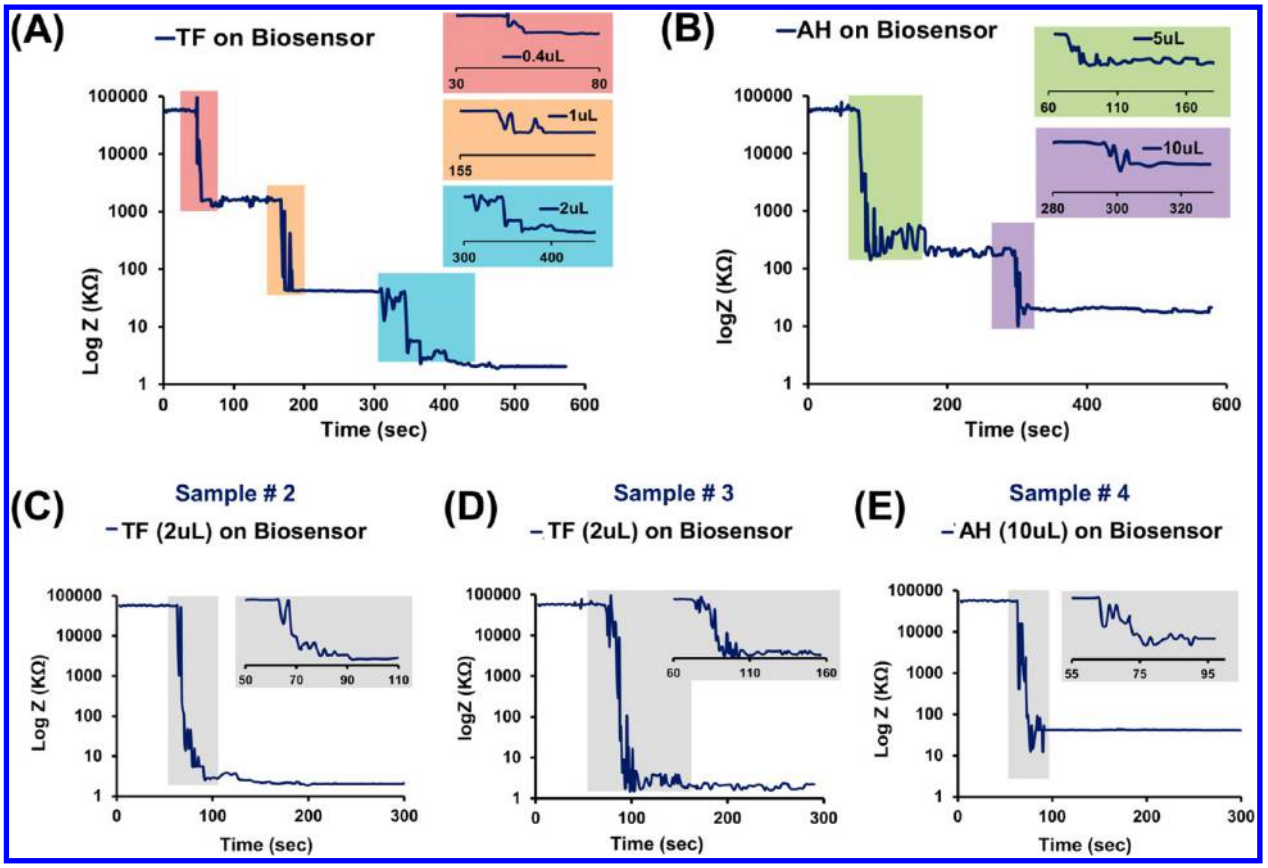

Figure 8. Performance, real-time monitoring, and system stability of the developed ocular biosensor chip against clinically collected TF and AH at different volumes. (A) Impedance evaluation for continuous monitoring of TF with variable volume (0.4, 1, and 2 μL) on biosensor chip. (B) Impedance evaluation for continuous monitoring of AH with variable volume of 5 and 10 μL on biosensor chip. Individual response trends of TF with volume of (C) 1 and (D) 2 μL and (E) AH with volume of 10 μL loaded to ocular biosensor. Inset of each figure represents the steady state response of the TF under investigation at different volumes of TF and AH.

continuous real-time loading of TF sample on the same biosensor chip without disconnecting from the potentiostat. Finally, monitoring of electrochemical response of 2 μL for two different samples (no. 2 and 3) onto the biosensor chip coated with AO enzyme of 5 μL was also investigated. In these cases, biosensor chip exhibited the steady state response in ∼30 and 40 s as shown in Figures 8C and 8D, respectively.

Quantification of AA in Aqueous Humor. Real-time monitoring of AH with volume of 5 and 10 μL were tested directly onto ocular biosensor chip as shown in Figures 8B and 8E. In both cases, data were monitored until the system obtained steady state response with respect to electrical impedance. In Figure 8B, experiment was demonstrated in real-time fashion with continuous increase in volume of AH sample from 5 to 10 μL in two steps. After treating electrically assembled biosensor chip with 5 μL of AH, the biosensor's impedance subsequently decreased from 5.5 ± 0.06 to 217.5 ± 6.8 KΩ after 70 s (green highlighted area). With additional volume of 5 μL of AH on the same biosensor chip, it showed the steady state result within 20 s (purple highlighted area) with further reduction in impedance from 217.5 ± 6.8 to 20.6 KΩ. This represents the decrease in impedance of the chip after increasing the volume of the AH sample. This data reveals that AH sample with total volume of 10 μL showed a quick response as compared to 5 μL. In another experiment, we tested the same sample of AH (10 μL) clinically collected from the patient (sample 4 as shown in Figure 8E) with new biosensor chip conjugated with similar volume of enzyme AO (10 μL). We observed the similar trend that the impedance was dramatically decreased from 5.5 MΩ to 20.1 KΩ, and the steady state response was obtained within 35 s. This reveals that ocular biosensor has high probability (>0.95, n = 14) to achieve stabilization reading in less than 40 s with the approximate sample volume of 10 μL.

Analysis of Standard AA Solution and Estimation of AA in TF and AH. For AA detection process in TF and AH, a calibration curve was generated by measuring the change in impedance of the biosensor chip loaded with known concentration of AA standard solution. These experiments were carried out under the same conditions as described for TF an AH using three-electrode configuration potentiostat. The change in impedance was continuously monitored after dropping the AA sample with known concentration (5, 10, 100, and 1000 μM) directly onto the sensing area of the biosensor chip. Base impedance of electrical biosensor chip was 5.5 MΩ. An AO enzyme (5 μL) was added onto the biosensor chip followed by standard AA (2 μL of 5 μM solution). This decreased the impedance of the sensor chip as shown in Figure 9A. Here, impedance of 13.5 KΩ shows the change of impedance occurred after treating the sensing area of the chip with AA solution with known concentration (5 μM) for 2 μL only. Biosensor chip exhibited the change in impedance up to 400 μM concentration of AA, and there was negligible change in impedance afterward. Similarly, change in impedance of 800 KΩ was revealed after treating the biosensor chip with standard AA (10 μL of 5 μM solution). For AH measurements, AO

DOI: 10.1021/acsami.7b01675
ACS Appl. Mater. Interfaces 2017, 9, 8609−8622

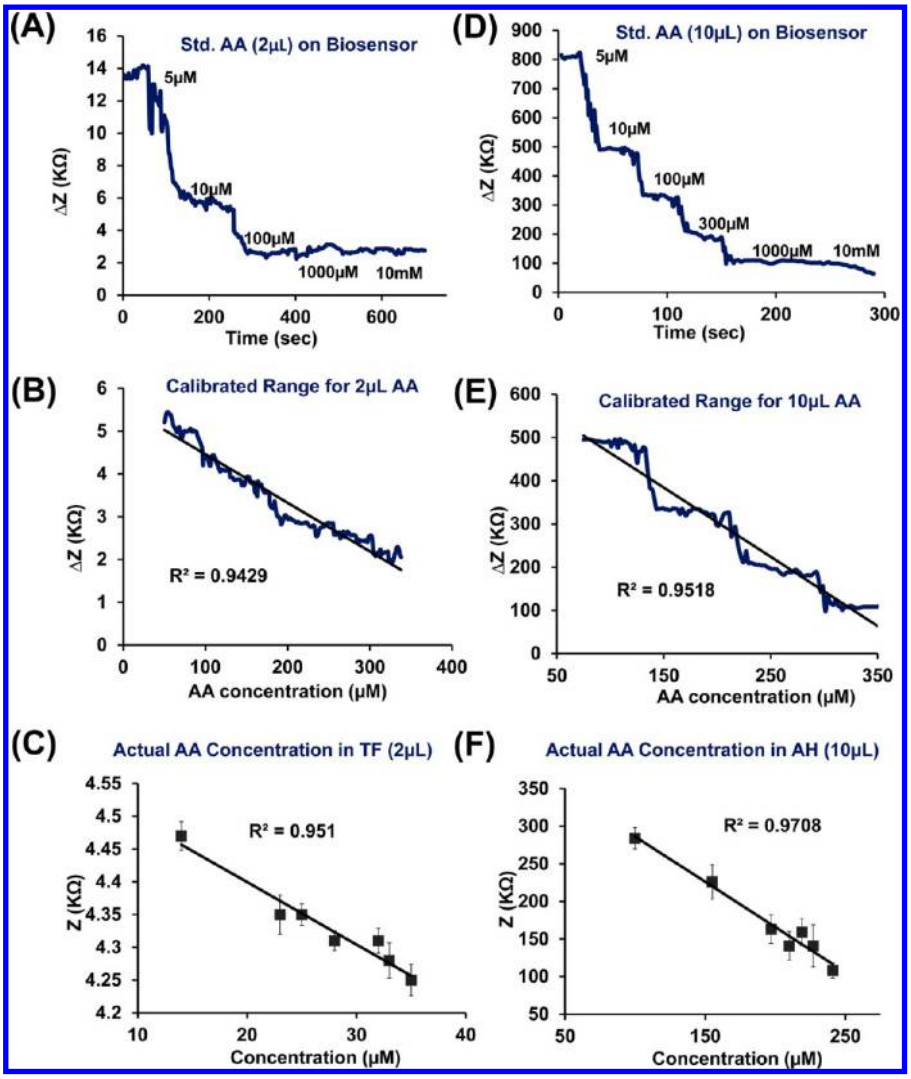

Figure 9. Standard AA solution with different concentrations and normalized impedance data for TF (2 μL) and AH (10 μL) samples. (A) Real-time monitoring of sequential addition of standard AA at different concentrations for 2 μL. (B) Calibrated range for 2 μL sample on ocular biosensor for estimation of AA in TF. (C) Estimation of AA concentration in TF samples using calibration curve of standard AA solution. (D) Real-time monitoring of sequential addition of standard AA at different concentrations for 5 μL. (E) Calibrated range for 10 μL sample on ocular biosensor for estimation of AA in AH. (F) Estimation of AA concentration in AH samples using calibration curve of standard AA solution.

enzyme with volume of 10 μL was conjugated. In this case, due to large volume of AO and AH, biosensor chip showed the change in impedance up to 1000 μM concentration of AA, and there was no change afterward as shown in Figure 9D. Figures 9B and 9E revealed the calibration of the biosensor chip after treating with 2 and 10 μL samples of AA. Regression value of 0.9429 and 0.9518 were achieved for standard AA concentration ranging from 5 to 350 μM.

The final calibration equation was plotted on the experimental data after comparing the results of TF and AH with standard AA solution. Estimated impedance data followed a linear trend with regression value (R^2) of 0.951 for TF and 0.971 for AH as shown in Figures 9C and 9F, respectively. The concentration of AA in unknown AH and TF sample was estimated using the calibrated linear fit. The average values of quantified AA in AH and TF were found be consistent and reproducible as tabulated in Tables S1 and S2. Results revealed a clear correlation between standard AA and AA levels presence in AH and in TR, but the ratio varied in samples for different subjects, probably due to difference in tear production rate. A full thickness laceration in the cornea or anterior scleral from trauma or incisional surgery could release AH into the TF which pathologically increases the concentration of AA in TF to a significantly higher level than that found in normal eyes. It was found that the level of AA in AH from seven subjects were ranging from 110 to 225 μM, whereas TF samples from eight subjects were found to be in the range 15−38 μM, which was in commensurate with the range of normal conditions. The reproducibility of ocular biosensor for AA level detection in TF and AH was investigated through the repeated trials. This study confirmed the possibility of detecting AA in TF of subjects with eye injuries or patients after surgery using this ocular biosensor chip. This potential information could then be used to evaluate wounds leaks in terms of severity level. Higher severity leaks would refer to high AA concentration in the tear film.

Sensitivity, Accuracy, Shelf Life, and Bland−Altman Analysis of Biosensor Chip. The developed biosensor chip exhibited a lower detection limit to be 4.93 ± 0.53 and 39.63 ± 4.4 ng/μL for TF and AH samples, respectively. The team has presented the sensitivity of 88% (n = 8) after comparison with

DOI: 10.1021/acsami.7b01675
ACS Appl. Mater. Interfaces 2017, 9, 8609−8622

standard calorimetric assay (AA Assay Kit, Sigma-Aldrich, MAK074) test. To measure the concentration of AA in the clinical samples, 5 μL of AH sample was added to the master mix (50 μL) and buffer (140 μL) to obtain the absorbance/fluorescence data. Standard AA with known concentrations of 100, 200, 350, 500, and 1000 μM was used. Results presented in Table S3 showed the concentration of AA in AH with large sample volume of 10−20 μL. There is no comparison of colorimetric assay technique with the developed biosensor chip to measure the concentration of AA in TF sample with low volume in the range of 0.5−2 μL. The colorimetric assay is a current laboratory method for testing AA concentrations. This cannot be done in a point-of-care fashion. This test was only used in the case of aqueous humor with large volume. The tear film sample is too small of a quantity to use the colorimetric test for a standard comparison. In the work, we present that ocular biosensor chip has the ability to read the presence of AA in TF sample even with volume of 400 nL, which is unique from competitors. The standard colorimetric assay alone demonstrated the sensitivity of 92%. So, there is essentially a difference of ∼4% between our technique and the colorimetric assay. Standard colorimetric assay was used extensively to confirm the accuracy of the developed biosensor chip. The colorimetric assay is a current laboratory method for testing AA concentrations. This cannot be done in a point-of-care fashion. Here, we would like to point out that the feasibility of running a colorimetric assay using tear fluid is none due to the requirement of a high volume of samples for the assay. The standard assay can only be used in the case of aqueous humor where collecting large sample volume is feasible. Consequently, for tear fluid analysis, the measurement of AA in TF with any standard colorimetric assay was not possible because it required at least 20 μL sample volume to be analyzed. Moreover, the calibration curve was generated using standard AA samples with known concentration (Figure 9) followed by a comparison of the results with clinical samples (TF and AH with unknown AA concentration (Figure 8)) using the biosensor chip.

To study the shelf life of the ocular biosensor chip, measurements were taken at intervals of 1 week (Figure S7a). The results show that multilayered electrical biosensor chip exhibited stable performance for up to 4 weeks. Beyond that time the electrochemical response of polymer−graphene composite was significantly reduced and could not produce the effective outcome to determine ascorbic acid concentration accurately. Error bars represent the relative standard deviation for three samples used to evaluate the shelf life. Finally, Bland−Altman analysis was done to estimate the agreement between two quantification methods of AA detection for AH samples: colorimetric assay and ocular biosensor (Figure S7b). The Bland−Altman plot was obtained by plotting the difference between concentrations measured from two methods (ocular and colorimetric assay) with the mean of the concentrations measured by the two methods. It generated a bias value of −19.625 μM, which indicates that the sensor under predicted the AA concentration compared to the gold standard colorimetric assay. This may be due to the oxidation of AA during sample handling and experimentation. The goal of this article was to develop an electrical biosensor chip that can provide quantitative detection of AA and to test the feasibility of analysis using a very small volume of sample. When we translate this technology to clinics, the sample collection will be directly integrated with the sensor. Direct integration of the sample collection device with the sensor will avoid the undesired oxidation of AA. This approach will remove the pretreatment procedure which caused oxidation of ascorbic acid during sample handling and experiment. The limit of agreement (95% confidence interval, CI) was calculated and plotted for from eight samples (n = 8) analyzed on the ocular biosensor and the colorimetric assay.

Empathic Design of a Hand-Held Probe. Industrial empathic product design research and testing with robust prototype evaluation was focused upon use of materials, patient needs, ease of use, scale, location of device when not in use, and product protocols. The device design was refined to integrate the technology into a preproduction working prototype that can be evaluated and tested for the next stage of the development process. A human-centric design approach was pursued, which was driven by the needs of both patient and medical professionals.

The initial empathic design research phase began with observing eye specialists as they perform the ocular examination. Observations were made on the use of the current tool, comfort with holding instruments, and approach to the patients. Observing each step from the initial patient consultation to the final examination helped us to determine the product category language and use of visual semantics (e.g., the current standard forms and signage), context environment, and stages of various tasks involved with eye examinations. The focus was based on authentic human behavior of the medical specialists, and therefore, body language, microfacial expressions, what is spoken, and what is not discussed to contribute to understanding the functional and suprafunctional (e.g., emotional and cultural) needs[52,53] were considered. This helped to elicit visual cues, pattern of behavior, and product design opportunities.

A critical comparative evaluation was performed to provide a breakdown of the device used with ocular surface testing (e.g., Tonopen, Reichert Inc., Buffalo, NY, and the OcuSense TearLab, San Diego, CA) to better understand their specific qualities. The Tonopen is a portable hand-held device that measures eye pressure. It was initially accepted into most emergency room and eye departments as a tool that provided an easier method for measuring eye pressure. However, due to design flaws including frequent need for calibration, short battery life, and difficulty with stabilizing the device in testing, the Tonopen is being replaced by competing devices forcing Reichert to redesign the product. This underscores the importance of correct design modeling and empathetic research investigations in early prototype design. Our design included (i) ease of use, (ii) opportunities to reduce stages of tasks to improve efficiency, and (iii) common visual language. This would ensure the design outcome sits well in the intended environment, which contributes to it being more intuitive to engage with even when new to the user. These help to modify construction and design of the final device.

Once the product design specifications (e.g., acceptable weight, anthropometric constraints, device overall size, form variations) were defined, sketching was performed as shown in Figure S4a. Low-fidelity three-dimensional models were developed from the two- and three-dimensional sketches of the ocular biosensor that will accommodate the anthropometric data of users. We focused on advanced visualization of concepts, pen renderings, CAD renderings, and three-dimensional physical models.

DOI: 10.1021/acsami.7b01675
ACS Appl. Mater. Interfaces 2017, 9, 8609−8622

3. EXPERIMENTAL SECTION

Preparation of Graphene Nanoplatelet and PS-*b*-PAA Composite. Graphene nanoplatelets (GP, 100 mg, 10 mg/mL) were mixed with polystyrene-*block*-poly(acrylic acid) (PS-*b*-PAA) amphiphilic polymer suspension (10 mg, 1.0 mg/mL) in 10 mL of DI water. Graphene nanoplatelets and PS-*b*-PAA were purchased from STERN Chemicals, USA, and Sigma-Aldrich, Saint Louis, MO, respectively. The mixture (GP−polymer) was probe sonicated at amplitude 4, with pulse of 5 s on and 1 s off for 4 h with intermittent cycles of 30 min. Process was completed at controlled temperature of 60 °C. To increase the uniformity of GP composite over paper, a spin-coating technique was used. Whatman filter paper of diameter 5 cm was used to be coated with GP composite by the spin-coating technique. Samples were dried using nitrogen spray gun for 10 min and were further dried overnight under biosafety hood at room temperature to maintain sterility. Ascorbate oxidase enzyme was then immobilized using the drop-cast method directly on the sensing area for the measurements. Enzyme-coated papers were incubated at room temperature for 2.5 h under germ-free conditions for air drying before treating with clinically collected samples of tear film (TF) and aqueous humor (AH).

Fabrication of Contour-Based μ-Electrodes. The contour-based μ-electrode (CBμE) was fabricated directly on the thin layer of GP composite using a shadow mask to avoid laborious and complex optical lithography process. The design of electrodes (CBμE) was initially created in AutoCAD and used to develop a shadow mask on nickel brass with thickness of 0.025 mm by Photo Sciences Inc., Torrance, CA. A uniform layer of gold metal with a thickness of 40 nm was deposited using CHA E-Beam Evaporation System at Micro Nano Technology Laboratory (MNTL) facility, UIUC.

Scanning Electron Microscopy. For SEM imaging, the developed biosensor squares were loaded to the SEM sample holder using a piece of carbon tape. The images were obtained using a Hitachi (Schaumburg, Illinois) S-4700 SEM with Oxford Instruments (Abingdon, Oxfordshire). Imaging was performed in a long working distance mode, with an accelerating voltage of 10 kV, extracting current of 10 μA, and working distance of 25 mm for scanning.

Atomic Force Microscopy. For AFM analysis, a square of biosensor strip was pasted to a steel slide using a double-sided tape. AFM images were obtained using an Asylum Cypher (Santa Barbara, CA) with tapping mode and phase mode. The surface of strip was scanned in air using OMCL-AC160TS cantilevers at a set point of 0.63 V, 1 Hz scan rate, and drive frequency of 336.3 kHz.

Raman Spectroscopy. All Raman measurements were taken on a Nanophoton Raman instrument with a 532 nm wavelength laser. For each spectrum a grating (600 lines mm^{-1}) scan was taken over the range of 120−2700 cm^{-1}. Point scans were performed at 0.2% laser power for 1 min using a 20× objective. An average of 20 spectra were recorded and averaged per sample. For Raman micrographs, samples were imaged using line scans at 20% laser power and a 5× objective at rate of 20 s per scan.

X-ray Diffraction. The crystallographic features of the fabricated electrodes and polymer were examined by X-ray diffractometry, XRD (Siemens- Bruker D5000, Madison, WI), using Cu Kα radiation in the θ−2θ. The samples were mounted on a glass slide and were raised using clay to level the sample on the holder.

NMR. ^{1}H NMR measurements were performed on VARIAN UNITY 500 (Varian, Inc., Palo Alto, CA) spectrometer operating at 500 MHz equipped with 5 mm Nalorac QUAD probe at Roger Adams Laboratory, UIUC. Chemical shifts were reported in ppm and referenced to the solvent proton impurities. Deuterium oxide (D_2O) was used as the deuterated solvent for all samples. 600 μL of sample was transferred to the NMR tube. A total of 256 acquisitions were made, and the data were processed and analyzed with MestRenova 8.1 software (Mestrelab Research SL; Santiago de Compostela, Spain).

X-ray Photoluminescent Spectrum. X-ray photoluminescent spectrum (XPS) was obtained on the fabricated chip before and after the application of AA on the AO deposited sample. A Physical Electronics PHI 5400 spectrometer was used equipped with Al Kα (1486.6 eV) radiation lamp. The spectrum was referenced to the adventitious C 1s feature at 284.8 eV. The data were analyzed with referring to the NIST database.

Mass Spectrometry. A standard ascorbic acid (AA) sample was purchased from Sigma-Aldrich and was used without purification. LC-HRMS was performed on a Waters Synapt G2Si mass spectrometer. The column model used was ACQUITY UPLC BEH C18, 1.7 μm, 2.1 mm × 50 mm. Mobile phase A was 95% H_2O, 5% CAN, 0.1% FA, and mobile phase B was 5% H_2O, 95% CAN, 0.1% FA. The linear gradient sequence is 100% A, 0% B (0.5 min), 20% A, 80% B (4.0 min), and 100% A, 0% B (4.1 min) with the flow rates at 0.3 mL/min. The autosampler temperature was at room temperature. Negative mass spectrometry and the electrospray ionization (ESI) method were used to acquire the data. A 2000 V of voltage was used for ion spray, and the source temperature was kept at 400 °C.

Aqueous Humor (AH) and Tear Film (TF) Sample Collection Procedure. AH samples were collected from patients with localized retinal detachments who were scheduled for paracentesis to release intraocular pressure after therapeutic pneumatic retinopexy for localized retinal detachments, which is the standard of care. The procedure was performed in a clinical setting after placement of a topical anesthetic drop of proparacaine and antibiotic drop of ocufloxacin on the cornea of each patient. The fluid was collected using a sterile 30-gauge needle attached to a sterile 1 mL syringe. After collection, the needle was removed and discarded in the appropriate sharps container for disposal, and the syringe containing the fluid sample was then capped and placed in a biohazard specimen collection bag supplied by the hospital. No patient identifiers were connected to the sample. For TF sample collection, a small disposable glass capillary tube was placed in the tear lake that forms on the lower eyelid, and the fluid was passively obtained by capillary action. A member of the research team brought the samples (TF and AH) to the research laboratory at the Mills Research Center for further testing. The Ophthalmology Department at Carle is directly connected to the research laboratory by the use of a walkway between the buildings.

4. CONCLUSIONS

The change in impedance of the graphene platelet−ascorbate oxidase assembly due to presence of different concentration of AA was measured using a potentiostat with a three-electrode configuration connected to a data acquisition system. The AA concentration within TF and AH were monitored by our novel point-of-care device. Data were continuously acquired after dropping the clinically collected samples on the sensor until measurement stabilized. Since AA concentration is documented to be higher within the aqueous fluid of tear film, we anticipate that an increase in AA presence within the tear film can also be used to monitor the integrity of cornea and anterior scleral wounds in postoperative management of ophthalmic patients. The potential impact of this study will be a significant change in the current method for evaluating eye postsurgical patients as well as trauma patients. It will improve the utilization of health care resources and quality of eyecare for patients. The quantitative reading will be used to grade the severity of a wound leak, and treatment will be personalized for the patient based on the severity discovered by the proposed electrical biosensor chip in this work. Ease-of-use and portability will make the biosensor a perfect hand-held device for use in the clinical settings. We anticipate that the sensor could detect wound leaks more sensitively and accurately than current options.

■ ASSOCIATED CONTENT

Supporting Information

The Supporting Information is available free of charge on the ACS Publications website at DOI: 10.1021/acsami.7b01675.

DOI: 10.1021/acsami.7b01675
ACS Appl. Mater. Interfaces 2017, 9, 8609−8622

Additional text, seven figures, and three tables have been included to further demonstrate the layer-by-layer description, experimental setup of biopotentiostat connectivity, spin-coating of graphene−polymer on paper and shelf life of ocular biosensor chip; additional characterization has been included using SEM, NMR, and XPS (PDF)

AUTHOR INFORMATION

Corresponding Author

*E-mail dipanjan@illinois.edu (D.P.).

ORCID

Dipanjan Pan: 0000-0003-0175-4704

Notes

The authors declare the following competing financial interest(s): Prof. Pan and Dr. Labriola are the co-founders of InnSight, Inc. a start-up company, which did not fund this research.

ACKNOWLEDGMENTS

SEM, AFM, XRD, XPS, and Raman images/data were acquired at Frederick Seitz Materials Research Laboratory (MRL) Central research facilities, UIUC. Fabrication of μ-electrodes was performed at Micro-Nanotechnology Laboratory (MNTL) facility, UIUC. NMR experiment was done at Rogers Adam Laboratory at UIUC. LC-HRMS was demonstrated at Noyes Laboratory, School of Chemical Sciences (SCS) at UIUC. Authors specially acknowledge Mr. Simpson Burt, a graduate student at SCS, UIUC for his help in arranging the CH Instruments 760E biopotentiostat to do initial electrical measurements. All clinical samples (tear film and aqueous humor) were collected at Eye Clinic of Carle Foundation Hospital, Urbana, IL. Authors gratefully acknowledge funding from NSF Award 1548915, University of Illinois at Urbana−Champaign, Children's Discovery Institute and Institute of Sustainability in Energy and Environment.

REFERENCES

(1) Meskin, S. W.; Ritterband, D. C.; Shapiro, D. E.; Kusmierczyk, J.; Schneider, S. S.; Seedor, J. A.; Koplin, R. S. Liquid Bandage (2-Octyl Cyanoacrylate) as a Temporary Wound Barrier in Clear Corneal Cataract Surgery. *Ophthalmology* **2005**, *112*, 2015−2021.

(2) Bresson-Dumont, H.; Lehoux, A.; Foucher, J. Long Term Follow-Up of Bleb Reconstruction After Glaucoma Filtering Surgery. *J. Fr. D Ophtalmol.* **2009**, *32*, 241−246.

(3) Calladine, D.; Ward, M.; Packard, R. Adherent Ocular Bandage for Clear Corneal Incisions Used in Cataract Surgery. *J. Cataract Refractive Surg.* **2010**, *36*, 1839−1848.

(4) Hayashi, K.; Tsuru, T.; Yoshida, M.; Hirata, A. Intraocular Pressure and Wound Status in Eyes Immediately After Scleral Tunnel Incision and Clear Corneal Incision Cataract Surgery. *Am. J. Ophthalmol.* **2014**, *158*, 232−241.

(5) Kirwan, J. F.; Lockwood, A. J.; Shah, P.; Macleod, A.; Broadway, D. C.; King, A. J.; Mcnaught, A. I.; Agrawal, P. Trabeculectomy in the 21st Century: A Multicenter Analysis. *Ophthalmology* **2013**, *120*, 2532−2539.

(6) Leite, M. T.; Prata, T. S.; Kera, C. Z.; Miranda, D. V.; De Moraes Barros, S. B.; Melo, L. A. S. Ascorbic Acid Concentration is Reduced in the Secondary Aqueous Humour of Glaucomatous Patients. *Clin. Exp. Ophthalmol.* **2009**, *37*, 402−406.

(7) Song, A.; Scott, I. U.; Flynn, M. P. H. H. W.; Budenz, D. L. Delayed-Onset Bleb-Associated Endophthalmitis: Clinical Features and Visual Acuity Outcomes. *Ophthalmology* **2002**, *109*, 985−991.

(8) Mac, I.; Soltau, J. B. Glaucoma-Filtering Bleb Infections. *Curr. Opin. Ophthalmol.* **2003**, *14*, 91−94.

(9) Leng, T.; Miller, D.; Flynn, H. W.; Jacobs, D. J.; Gedde, S. J. Delayed-Onset Bleb-Associated Endophthalmitis (1996−2008): Causative Organisms and Visual Acuity Outcomes. *Retina* **2011**, *31*, 344−352.

(10) Thoms, S. S.; Musch, D. C.; Soong, H. K. Postoperative Endophthalmitis Associated with Sutured Versus Unsutured Clear Corneal Cataract Incisions. *Br. J. Ophthalmol.* **2007**, *91*, 728−730.

(11) Klein, R.; Klein, B. E. K. The Prevalence of Age-Related Eye Diseases and Visual Impairment in Aging: Current Estimates. *Invest. Ophthalmol. Visual Sci.* **2013**, *54*, ORSF5.

(12) Yamada, H.; Sawada, A.; Kuwayama, Y.; Yamamoto, T. Blindness Following Bleb-Related Infection in Open Angle Glaucoma. *Jpn. J. Ophthalmol.* **2014**, *58*, 490−495.

(13) Bochmann, F.; Kaufmann, C.; Kipfer, A.; Thiel, M. A. Corneal Patch Graft for the Repair of Late-Onset Hypotony or Filtering Bleb Leak After Trabeculectomy: A New Surgical Technique. *J. Glaucoma* **2014**, *23*, e76−e80.

(14) Jampel, H. D.; Solus, J. F.; Tracey, P. A.; Gilbert, D. L.; Loyd, T. L.; Jefferys, J. L.; Quigley, H. A. Outcomes and Bleb-Related Complications of Trabeculectomy. *Ophthalmology* **2012**, *119*, 712−722.

(15) Rootman, D. B.; Kumar, N. L.; Rootman, D. S.; Trope, G. E. Buccal Mucous Membrane for the Reconstruction of Complicated Leaking Trabeculectomy Blebs. *J. Glaucoma* **2010**, *19*, 270−274.

(16) May, W. N.; Castro-Combs, J.; Quinto, G. G.; Kashiwabuchi, R.; Gower, E. W.; Behrens, A. Standardized Seidel Test to Evaluate Different Sutureless Cataract Incision Configurations. *J. Cataract Refractive Surg.* **2010**, *36*, 1011−1017.

(17) Holly, F. J. Tear Film Physiology. *Am. J. Optom. Physiol. Opt.* **1980**, *57*, 252−257.

(18) Braun, R. J. Dynamics of the Tear Film. *Annu. Rev. Fluid Mech.* **2012**, *44*, 267−297.

(19) Begley, C.; Simpson, T.; Liu, H.; Salvo, E.; Wu, Z.; Bradley, A.; Situ, P. Quantitative Analysis of Tear Film Fluorescence and Discomfort During Tear Film Instability and Thinning. *Invest. Ophthalmol. Visual Sci.* **2013**, *54*, 2645−2653.

(20) Jagota, S. K.; Dani, H. M. A New Colorimetric Technique for the Estimation of Vitamin C Using Folin Phenol Reagent. *Anal. Biochem.* **1982**, *127*, 178−182.

(21) Kyaw, A. A Simple Colorimetric Method for Ascorbic Acid Determination in Blood Plasma. *Clin. Chim. Acta* **1978**, *86*, 153−157.

(22) Voif, I.; Gerhard, P.; Moeslinger, T.; Brunner, M.; Volf, I.; Spieckermann, P. G. Spectrophotometric Determination of Ascorbic Acid and Dehydroascorbic Acid. *Clin. Chem.* **1995**, *41*, 1177−1181.

(23) Nejati-Yazdinejad, M. Indirect Determination of Ascorbic Acid (Vitamin C) By Spectrophotometric Method. *Int. J. Food Sci. Technol.* **2007**, *42*, 1402−1407.

(24) Ferin, R.; Pavão, M. L.; Baptista, J. Rapid, Sensitive and Simultaneous Determination of Ascorbic and Uric Acids in Human Plasma by Ion-Exclusion HPLC-UV. *Clin. Biochem.* **2013**, *46*, 665−669.

(25) Kandar, R.; Drabkova, P.; Hampl, R. The Determination of Ascorbic Acid and Uric Acid in Human Seminal Plasma Using an HPLC with UV Detection. *J. Chromatogr. B: Anal. Technol. Biomed. Life Sci.* **2011**, *879*, 2834−2839.

(26) Romeu-Nadal, M.; Morera-Pons, S.; Castellote, A. I.; Lopez-Sabater, M. C. Rapid High-Performance Liquid Chromatographic Method for Vitamin C Determination in Human Milk Versus an Enzymatic Method. *J. Chromatogr. B: Anal. Technol. Biomed. Life Sci.* **2006**, *830*, 41−46.

(27) Gazdik, Z.; Zitka, O.; Petrlova, J.; Adam, V.; Zehnalek, J.; Horna, A.; Reznicek, V.; Beklova, M.; Kizek, R. Determination of Vitamin C (Ascorbic Acid) Using High Performance Liquid Chromatography Coupled with Electrochemical Detection. *Sensors* **2008**, *8*, 7097−7112.

(28) Zhu, S.; Li, H.; Niu, W.; Xu, G. Simultaneous Electrochemical Determination of Uric Acid, Dopamine, and Ascorbic Acid at Single-

DOI: 10.1021/acsami.7b01675
ACS Appl. Mater. Interfaces 2017, 9, 8609−8622

Walled Carbon Nanohorn Modified Glassy Carbon Electrode. *Biosens. Bioelectron.* **2009**, *25*, 940−943.
(29) Xiao, X.; Miller, P. R.; Narayan, R. J.; Brozik, S. M.; Wheeler, D. R.; Brener, I.; Wang, J.; Burckel, D. B.; Polsky, R. Simultaneous Detection of Dopamine, Ascorbic Acid and Uric Acid at Lithographically-Defined 3D Graphene Electrodes. *Electroanalysis* **2014**, *26*, 52−56.
(30) Sun, C. L.; Lee, H. H.; Yang, J. M.; Wu, C. C. The Simultaneous Electrochemical Detection of Ascorbic Acid, Dopamine, and Uric Acid Using Graphene/Size-Selected Pt Nanocomposites. *Biosens. Bioelectron.* **2011**, *26*, 3450−3455.
(31) Peik-See, T.; Pandikumar, A.; Nay-Ming, H.; Hong-Ngee, L.; Sulaiman, Y. Simultaneous Electrochemical Detection of Dopamine and Ascorbic Acid Using an Iron Oxide/Reduced Graphene Oxide Modified Glassy Carbon Electrode. *Sensors* **2014**, *14*, 15227−15243.
(32) Ngai, K. S.; Wee Tan, T.; Zainal, Z.; Zawawi, R. M.; Zidan, M. Voltammetry Detection of Ascorbic Acid at Glassy Carbon Electrode Modified By Single-Walled Carbon Nanotube/Zinc Oxide. *Int. J. Electrochem. Sci.* **2013**, *8*, 10557−10567.
(33) Kaur, B.; Pandiyan, T.; Satpati, B.; Srivastava, R. Simultaneous And Sensitive Determination of Ascorbic Acid, Dopamine, Uric Acid, And Tryptophan with Silver Nanoparticles-Decorated Reduced Graphene Oxide Modified Electrode. *Colloids Surf., B* **2013**, *111*, 97−106.
(34) Alwarappan, S.; Liu, G.; Li, C. Z. Simultaneous Detection of Dopamine, Ascorbic Acid, and Uric Acid at Electrochemically Pretreated Carbon Nanotube Biosensors. *Nanomedicine* **2010**, *6*, 52−57.
(35) Kim, Y.-R.; Bong, S.; Kang, Y.-J.; Yang, Y.; Mahajan, R. K.; Kim, J. S.; Kim, H. Electrochemical Detection of Dopamine in The Presence of Ascorbic Acid Using Graphene Modified Electrodes. *Biosens. Bioelectron.* **2010**, *25*, 2366−2369.
(36) Kuizenga, A.; Van Haeringen, N. J.; Kijlstra, A. Inhibition of Hydroxyl Radical Formation by Human Tears. *Invest. Ophthalmol. Vis. Sci.* **1987**, *28*, 305−313.
(37) Choy, C. K.; Benzie, I. F.; Cho, P. Ascorbic Acid Concentration and Total Antioxidant Activity of Human Tear Fluid Measured Using the FRASC Assay. *Invest. Ophthalmol. Vis. Sci.* **2000**, *41*, 3293−3298.
(38) Gogia, R.; Richer, S. P.; Rose, R. C. Tear Fluid Content of Electrochemically Active Components Including Water Soluble Antioxidants. *Curr. Eye Res.* **1998**, *17*, 257−263.
(39) Paterson, C. A.; O'Rourke, M. C. Vitamin C Levels in Human Tears. *Arch. Ophthalmol.* **1987**, *105*, 376−377.
(40) Howard, R. R.; Peterson, T.; Kastl, P. R. High-Performance Liquid Chromatographic Determination of Ascorbic Acid in Human Tears. *J. Chromatogr., Biomed. Appl.* **1987**, *414*, 434−439.
(41) Van Setten, G.-B.; Stephens, R.; Tervo, T.; Salonen, E.-M.; Tarkkanen, A.; Vaheri, A. Effects of the Schirmer Test on the Fibrinolytic System in the Tear Fluid. *Exp. Eye Res.* **1990**, *50*, 135−141.
(42) Reim, M.; Seidl, M.; Brucker, K. Accumulation of Ascorbic Acid in the Corneal Epithelium. *Ophthalmic Res.* **1978**, *10*, 135−139.
(43) Ringvold, A.; Anderssen, E.; Kjønniksen, I. Distribution of Ascorbate in the Anterior Bovine Eye. *Invest. Ophthalmol. Vis. Sci.* **2000**, *41*, 20−23.
(44) Jesionowski, T.; Zdarta, J.; Krajewska, B. Enzyme Immobilization by Adsorption: A Review. *Adsorption* **2014**, *20*, 801−821.
(45) Jagannadham, K. Thermal Conductivity of Copper-Graphene Composite Films Synthesized by Electrochemical Deposition with Exfoliated Graphene Platelets. *Metall. Mater. Trans. B* **2012**, *43*, 316−324.
(46) Hodkiewicz, J. Characterizing Carbon Materials with Raman Spectroscopy. *Prog. Mater. Sci.* **2005**, *50*, 929−961.
(47) Gartia, M. R.; Misra, S. K.; Ye, M.; Schwartz-Duval, A.; Plucinski, L.; Zhou, X.; Kellner, D.; Labriola, L. T.; Pan, D. Point-of-Service, Quantitative Analysis of Ascorbic Acid in Aqueous Humor for Evaluating Anterior Globe Integrity. *Sci. Rep.* **2015**, *5*, 16011.
(48) Shen, B.; Zhai, W.; Chen, C.; Lu, D.; Wang, J.; Zheng, W. Melt Blending In Situ Enhances the Interaction Between Polystyrene and Graphene Through Π-Π Stacking. *ACS Appl. Mater. Interfaces* **2011**, *3*, 3103−3109.
(49) Held, P. Quantitation of Peptides and Amino Acids with a Synergy HT Using UV Fluorescence. *Biotek Appl. Note* **2006**, 1−8.
(50) Messerschmidt, A.; Ladenstein, R.; Huber, R.; Bolognesi, M.; Avigliano, L.; Petruzzelli, R.; Rossi, A.; Finazzi-Agró, A. Refined Crystal Structure of Ascorbate Oxidase at 1.9 Å Resolution. *J. Mol. Biol.* **1992**, *224*, 179−205.
(51) Cowdrey, G.; Firth, M.; Moss, R.; Karim, A.; Thompson, G.; Firth, G. The Analysis of Aqueous Humor Constituents Using Capillary Zone Electrophoresis. *Exp. Eye Res.* **1998**, *67*, 449−455.
(52) Thomas, J.; Mcdonagh, D. Empathic Design: Research Strategies. *AMJ* **2013**, *6*, 1−6.
(53) Mcdonagh, D.; Denton, H.; Chapman, J. Design and Emotion. *J. Eng. Des.* **2009**, *20*, 433−435.

DOI: 10.1021/acsami.7b01675
ACS Appl. Mater. Interfaces 2017, 9, 8609−8622